ACS APPLIED MATERIALS & INTERFACES

Research Article

www.acsami.org

Sulfur-Doped Polyimide Photocatalyst with Enhanced Photocatalytic Activity under Visible Light Irradiation

Cuicui Wang,[†,‡] Yong Guo,[§] Yu Yang,[†,‡] Sheng Chu,[†,‡] Chenkun Zhou,[‡] Ying Wang,*[,†,‡,∥] and Zhigang Zou*[,†,∥]

[†]Eco-materials and Renewable Energy Research Center (ERERC), National Laboratory of Solid State Microstructures, Kunshan Innovation Institute of Nanjing University, Nanjing 210093, China

[‡]School of Chemistry and Chemical Engineering, Nanjing University, Nanjing 210093, China

[§]School of Environment, Nanjing University, Nanjing 210093, China

[∥]Jiangsu key laboratory for nanotechnology, Nanjing 210008, China

ABSTRACT: Sulfur-doped polyimide (SPI) photocatalysts were synthesized for the first time via an *in situ* thermal copolymerization method using sublimed sulfur (S_4) as a dopant. Sulfur doping not only extended the absorption range of polyimide (PI) for visible light but also enhanced the oxidation ability of the photoinduced hole. The doped sulfur substitutes for the lattice nitrogen in triazine rings of PI to form the S−C bond and changes the distribution of negative charge in the two-dimensional plane of PI. The enhanced photocatalytic activity of SPI in the degradation of methyl orange is ascribed to the strong oxidation ability of the photoinduced hole of SPI and an effective suppression to the recombination of electrons and holes.

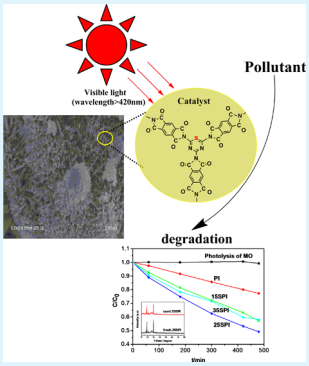

KEYWORDS: *sulfur doping, photocatalyst, polyimide, degradation, visible light*

1. INTRODUCTION

Utilizing renewable solar energy to clean serious environmental pollution is a significant topic. A key step to solving this intractable problem is to develop novel photocatalytic materials. Recently, some polymer semiconductor photocatalysts such as g-C_3N_4 and polyimide (PI) were found to efficiently degrade organic pollutants and split water to generate hydrogen under visible light.[1−4] These materials have attracted attention because these metal-free photocatalysts possess unique chemical stability, have a lower production cost, and are especially capable of utilizing solar energy. Much effort was then focused on further extending the adsorption of these materials for visible light and modifying the electronic band structure to enhance their photocatalytic performance. So far, chemical doping nonmetal elements such as P, F, or S in g-C_3N_4 have been reported to be an effective strategy for improving its photocatalytic activity.[5−8] Among them, the most elusive dopant is element sulfur; its modulation of the optical absorption property and electronic band structure of g-C_3N_4 is very dependent on the type of sulfur precursor and synthetic routes. Sulfur has been doped into the framework of g-C_3N_4 by post-treating g-C_3N_4 in a H_2S atmosphere;[7] it was found that the homogeneous substitution of sulfur for lattice nitrogen led to a widened valence band (VB) and an increase in the conduction band (CB) minimum (CB) of g-C_3N_4. A sulfur-doped mesoporous g-C_3N_4 (mpgCNS) was synthesized by *in situ* polymerization of thiourea with SiO_2 as a hard template, and a sulfur atom doped in the carbon position of mpgCNS, which resulted in downshifts of its CB and VB.[8] Wang and co-workers used sulfur-containing organic precursors (trithiocyanuric acid) to synthesize an innovative conjugated polymer composed of a disulfide (−S−S−) bond that was considered to play a key role in the light harvesting and electron transport capacity of the conjugated polymer.[9] They also found that introduction of sulfur heteroatoms into carbon nitride could lower the energy level of the VB and increase the O_2 evolution activity of the carbon nitride polymer semiconductor even when a very small amount of sulfur (∼0.5 wt %) remained in the resulting sample.[10] However, using a simple sulfur-containing compound such as thiourea, inorganic salt (ammonium thiocyanate), or elemental sulfur (S_8) as the precursor in sulfur-mediated synthesis identified the absence of S species in the resulting carbon nitride photocatalysts.[11−13] These results imply that the underlying cause of sulfur doping in modifying the electronic band structure and optical properties of polymer semiconductor photocatalysts is meaningful and deserves further inquiry. Previously, we have synthesized a donor−acceptor (D−A) polyimide (PI) photocatalyst by uniformly incorporating electron-deficient pyromellitic dianhydride (PMDA) blocks into the network of g-C_3N_4

Received: January 2, 2014
Accepted: March 3, 2014
Published: March 3, 2014

   dx.doi.org/10.1021/am500007u | *ACS Appl. Mater. Interfaces* 2014, 6, 4321−4328

via direct thermal condensation of melamine and PMDA at a mild temperature.[3] Compared with the uniform distribution of electronic charge on the two-dimensional (2D) framework of g-C_3N_4, the electronic charge distribution on this polyimide photocatalyst is "located" on the PMDA block because of the electron-deficient effect of PMDA, which implies a nonuniform distribution of electronic charge may lead to easy access for the dopant. Herein, we first report an S-doped polyimide (SPI) photocatalyst synthesized by *in situ* thermal polymerization of sublimed sulfur (S_4) and two monomers, melamine (MA) and PMDA, at mild temperatures. The resulting catalysts were carefully characterized by UV−vis, X-ray photoelectron spectroscopy (XPS), and valence band XPS (VBXPS) to study the location of sulfur in the framework of PI and the influence of sulfur doping on its optical properties and electronic band structure. The photocatalytic activity of SPI was assessed in the photodegradation of MO driven by visible light irradiation.

2. EXPERIMENTAL METHODS

2.1. Synthetic Procedure. Sublimed sulfur (S_4) was purchased from Nanjing Chemical. Melamine (MA) was obtained from Chengdu Kelong Chemical, and pyromellitic dianhydride (PMDA) was the product of Tixiai (Shanghai) Huacheng Industrial Development Co., Ltd. All reagents were directly used as received without further treatment.

Polyimide was synthesized by heating the mixture of 1.0 g of MA and 1.73 g of PMDA at 598 K for 4 h at a heating rate of 7 K/min in a semiclosed system; a yellow powder was obtained. Similarly, sulfur-mediated polyimide (SPI) was synthesized by heating the mixture of 1 g of MA, 1.73 g of PMDA, and 15, 25, and 35 wt % sublimed sulfur under the same synthetic condition that was used for PI. With different amounts of sulfur (S_4), dark yellow sulfur-mediated polyimides (SPIs) were obtained and are denoted 15SPI, 25SPI, and 35SPI, respectively.

2.2. Characterization. Power X-ray diffraction (PXRD) patterns of samples were obtained with the X-ray diffractomer (Rigaku Ultima III) with Cu Kα (λ = 1.540562 Å) radiation in the 2θ range from 10° to 80°, and the X-ray tube was operated at 40 kV and 40 mA. The scanning electron microscopy (SEM) image was recorded on a Hitachi S4800 FE-SEM system. The transmission electron microscopy (TEM) image was obtained on a JEM-2100 electron microscope.

The structural properties of 25SPI were measured using a BET measurement (Micromeritics-3000, Micrometrics) after 25SPI had been evacuated in the degas port at 373 K for 3 h. Fourier transform infrared (FT-IR) spectra of the samples were acquired on a Nicolet NEXUS870 spectrometer using the KBr pellet support, and UV−vis diffuse reflectance spectra of samples were measured on a Shimadzu UV 2550 spectrophotometer using $BaSO_4$ as a reference. XPS was performed with a PHE-5100X PSD instrument with an X-ray monochromator with standard Al and Mg Kα X-ray radiation. The resolution of the instrument was 0.8 eV, and the sensitivity was 80K counts per second. VBXPS was undertaken using a PHI 5000 Versa Probe photoelectron spectrometer with monochromatized Al Kα X-ray radiation. All binding energies were referenced to the C1s peak (284.6 eV) arising from adventitious carbon. Photoluminescence (PL) spectra were obtained at room temperature on a Varian Cary Eclipse fluorescence spectrometer with an excitation wavelength of 235 nm.

Theoretical calculations were performed with Gaussian 03. The B3LYP/6-31g method was used to optimize molecular models. All models were drawn with Gview based the B3LYP/6-31g-optimized results.

2.3. Photocatalytic Activity Evaluation. The photodegradation of MO in solution (4 mg/L) was conducted with visible light (wavelength of >420 nm) radiation, for which the 0.2 g sample was dispersed in 100 mL of an MO solution. The solution was irradiated with a 300 W Xe arc lamp (ILC Technology, CERMAX LX-300) with a 420 nm cutoff filter, while a water bath was used to keep the temperature constant. Before irradiation, the suspension was stirred for 1 h to reach the adsorption equilibrium. Then the lamp was turned on, and 3−4 mL of the reaction mixture was withdrawn at regular time intervals. All those collected mixtures were centrifuged and filtered through a 0.45 μm membrane filter to remove the catalyst particles. The obtained solution was analyzed with a UV−vis spectrometer. Because MO had the strongest absorbance at a wavelength of 463 nm, the concentration of the residual MO was ascertained by referring to the characteristic absorption of MO at 463 nm. The wavelength dependence experiment was performed on SPI by using the light source equipped with a long-pass filter during the 4 h reaction.

3. RESULTS AND DISCUSSION

PXRD patterns of pristine PI and sulfur-doped PI samples are displayed in Figure 1. As shown in Figure 1, several distinct

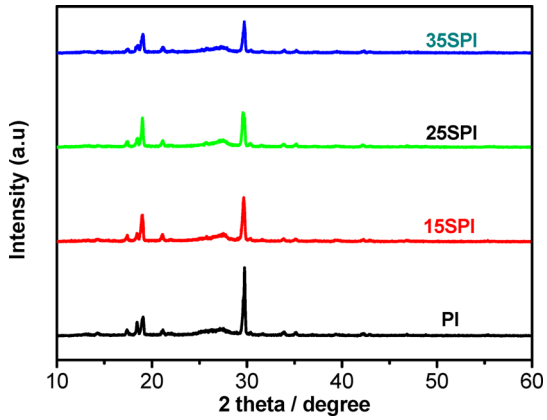

Figure 1. PXRD patterns of PI, 15SPI, 25SPI, and 35SPI.

peaks in the range of 10−30° clearly demonstrate the high crystallinity of the polymer samples, which indicates that the *in situ* synthesis of sulfur-doped PI crystalline by the one-pot thermally induced polycondensation method is very effective. It was noted that two diffraction peaks at 2θ values of 18° and 29.5° appear on the patterns of all sulfur-doped samples. Compared to that of pristine PI, similar peak features and no position shift of these peaks were observed, indicating sulfur doping did not change the original crystal structure or polymeric chain of PI. In contrast, the diffraction intensity of the peak at 29.5° apparently decreased with the amount of sulfur doping. Intriguingly, this phenomenon was also found on sulfur-doped C_3N_4 polymer semiconductors and ascribed to the reduction of the structural correlation length that was caused by a decrease in the size of the particle or spherical porogens.[7,8,14] For our polyimide samples, the crystalline growth can be ascribed to a typical thermal melt; the annealing polymerizing monomer component can greatly affect the crystalline texture of a polymer semiconductor, such as its chain orientation, framework ordering, and particle morphology. During the thermal polymerization, PMDA molecules first reach a molten state and react with adjacent MA molecules to form oligomeric polyimides,[3] and then these oligomers crystallize from the monomer melt with the aid of hydrogen bonding or $\pi-\pi$ electronic interaction between the conjugated core units, which results in a high degree of symmetry and regularity of polymer chains. In the synthesis of SPI, upon the addition of sublimed sulfur, the reaction system became more uniform because elemental sulfur acts as a molten flux to facilitate the polymerization of two monomers. On the other hand, partial sublimation and oxidation of sulfur in a static air atmosphere with the release of SO_2 and S during the reaction can inhibit the continuous growth of the oligomeric crystalline form, which

controls the particle size of SPI to some extent. The impact of sulfur doping on the morphology and particle size of PI will be further corroborated by SEM and TEM.

As demonstrated in the SEM image (Figure 2a), PI has a compact dendritic morphology with well-developed branches as

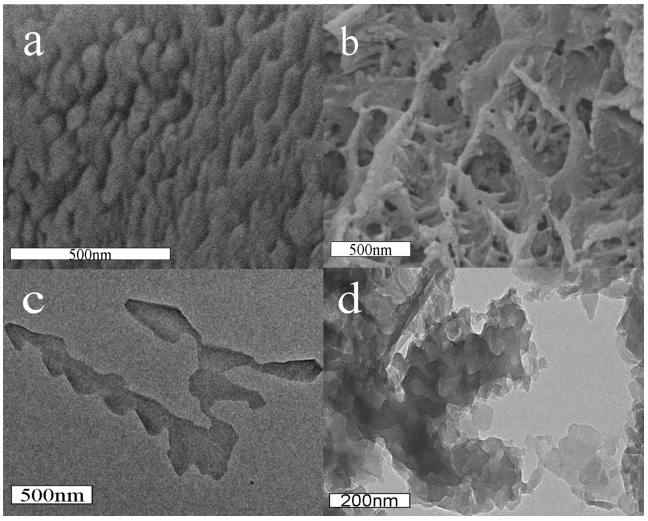

Figure 2. SEM (top) and TEM (down) images of PI (a and c) and 25SPI (b and d).

evidenced by TEM (Figure 2c). This special branched structure is the characteristic morphology of zigzag crystalline polyimides synthesized from a nonlinear molecule.[15] For the sulfur-doped sample of 25SPI, the loosening branched morphology with an obvious whisker structure and some irregular pores can be clearly discerned in its SEM image (Figure 2b), whereas the high-magnification TEM image of 25SPI illustrates that the branched whisker is aggregated by many small polyimide particles ~20 nm in diameter (Figure 2d). This effect of sulfur doping on the crystalline size of PI is in accordance with the weakening intensity of its XRD patterns (Figure 1).

Figure 3 illustrates the nitrogen adsorption−desorption isotherms of PI and 25SPI samples at 77 K. Both isotherms

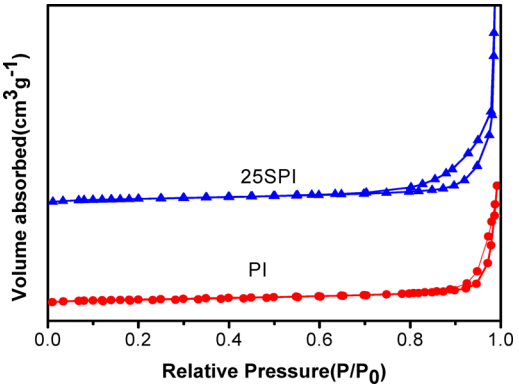

Figure 3. N_2 adsorption−desorption isotherms of 25SPI and PI.

possess a flat adsorption and desorption curve up to a relative pressure (P/P_0) of 0.8, mirroring the small amount of N_2 adsorbed at the lower relative pressure. When the relative pressure is increased to 0.8, a clear hysteresis loop appears in the isotherms of PI and 25SPI in the P/P_0 range of 0.8−1.0, representing the existence of mesopores. It is obvious that the hysteresis loop in the isotherm of PI is much smaller than that in 25SPI, and it is also slightly shifted toward the higher relative pressure (P/P_0 = 0.9−1.0), which indicates the larger pore volume and the more developed porous structure of the 25SPI composite, which coincided with its SEM image (Figure 2a). There has been speculation that those large pores on 25SPI probably resulted from the interconnected whisker. The different surface morphology of 25SPI and PI also results in the surface area of 25SPI (6.5 m^2/g) being slightly larger than that of PI (5.4 m^2/g). In the synthesis of 25SPI, sublimed sulfur was first melted as the solvothermal solvent to promote molecule diffusion, making the reactants easily contacted, and then a part of sulfur sublimed upon heating at a higher condensation temperature, which produces some irregular pores and/or channels in the resulting SPI composite.

FT-IR spectra of PI and SPI samples demonstrate the characteristic absorption bands mainly include few groups (Figure 4). The peaks marked with black solid lines around

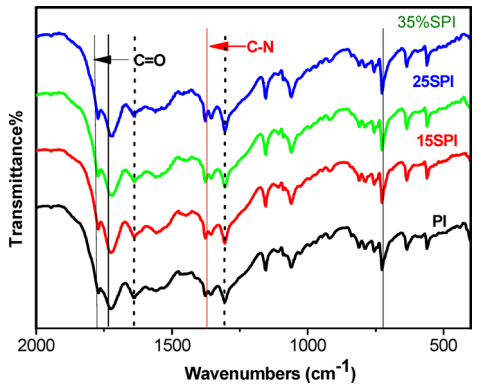

Figure 4. FT-IR spectra of PI and SPI samples.

1780, 1725, and 725 cm^{-1} are assigned to the stretching and bending vibrations of the −C═O bond in the PMDA moiety of PI.[16] The bands at 1560 and 1306 cm^{-1} marked with black dotted lines are indicative of the character of aromatic CN stretching and breathing modes in the triazine unit.[17] Compared with that in triazine-based frameworks of C_3N_4, the stretching vibration energy of the C−N bond in PI composites became strong because the electron-withdrawing PMDA blocks the substituent into the framework of C_3N_4. The band at 1376 cm^{-1} marked with a red line belongs to the characteristic vibratiog of the C−N−C bond in the five-membered imide rings.[18]

The several absorption bands at 1640 and 1157 cm^{-1} are contributed to the aromatic C−C and C−H bonds of benzene rings in dianhydride blocks.[19] Meanwhile, the several weak bands around 3200 cm^{-1} can be attributed to the amines and their intermolecular hydrogen bonds that are still present in the oligomeric building blocks; the intensities of these peaks become weaker as the amount of sulfur doping increases, implying sulfur-mediated synthesis promotes polymerization of MA and PMDA. Different from that reported on sulfur-doped carbon nitride polymers synthesized by using ammonium thiocyanate as the precursor,[12] the vibrating peak of the C−S bond at 480 cm^{-1} is weak in the spectrum of SPI, mirroring the amount of sulfur doping in PI being very small. In addition, no characteristic vibrating peak of the S−N bond in the range of 715−625 cm^{-1} is observed.[20] To further pursue the chemical environment and location of sulfur in the SPI sample, XSP

dx.doi.org/10.1021/am500007u | ACS Appl. Mater. Interfaces 2014, 6, 4321−4328

spectra of PI and the S doping sample were recorded at room temperature.

The existence of sulfur in the sample is confirmed by high-resolution S2p XPS spectra (Figure 5A). The binding energies

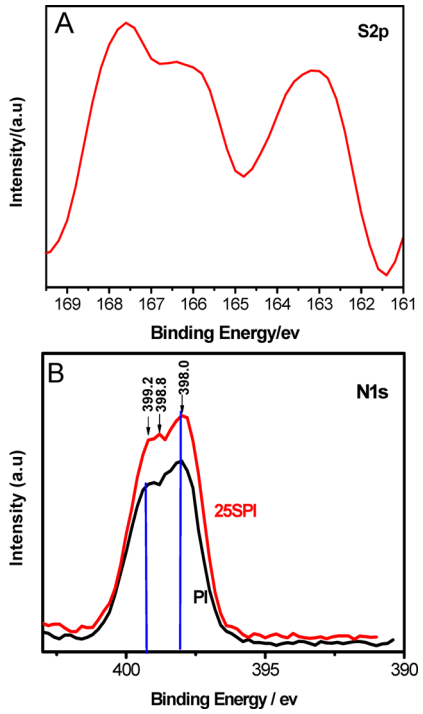

Figure 5. (A) S2p XPS spectrum of 25SPI and (B) N1s XPS spectra of PI and 25SPI samples.

of all the elements were referenced to the C1s peak (284.6 eV) arising from adventitious carbon. Three distinct S2p peaks appeared at binding energies of 163.3, 165.6, and 167.6 eV in the spectrum of 25SPI. These S2p binding energies are due to S2p3/2 core levels. The peak centered at 163.3 eV can be assigned to the $S2p_{3/2}$ signal of the C−S bond because the $S2p_{3/2}$ binding energy of CS_2 is approximate to this value.[21] Formation of C−S bands implies that doped sulfur substitutes the lattice N of triazine ring to form C−S bonds in SPI, as demonstrated in Scheme 1. Such a substitution of doped sulfur for the lattice N of the triazine ring was also found on sulfur-doped graphitic C_3N_4.[8,22] The shoulder peak at ∼165.6 eV tends to be ascribed to S−S bands[23] that arise from a small amount of residual sublimed sulfur absorbed on the surface of the sample. As for the peak at a high binding energy of 167.6 eV, it can be assigned to the sulfur oxide species (SO_4^{2-}) formed during the synthesis of SPI in an air atmosphere.[8,9] The amount of sulfur in 25SPI is 0.38 atom % based on the results of XPS analysis. TEM−EDS measurement was also performed to confirm the amount of doped sulfur in 25SPI; the value of 0.35 atom % is consistent. This is the first successful attempt to dope sulfur in the structure of a polymer semiconductor by using elemental sulfur (S_4) as the dopant precursor. Just as reported by a few groups, sulfur doping in the triazine rings of carbon nitride is very sensitive to the synthetic conditions. Using trithiocyanuric acid as a precursor could not produce a sulfur-doped carbon nitride photocatalyst above a polymeric temperature of 650 °C.[10] Sulfur-doped mesoporous g-C_3N_4 (mpgCNS) was synthesized by *in situ* polymerization by using thiourea as the sulfur precursor and SiO_2 as the template. The presence of sulfur was confirmed in the final sample and was proposed to substitute the position of carbon to form S−N bands in triazine rings.[9] However, using thiourea as a signal precursor without the SiO_2 template to synthesize g-C_3N_4 confirmed that no other sulfur species remained in the final samples.[11] Similarly, when the sulfur precursor was changed to elemental sulfur (S_8) for polymerization with melamine, XPS verified the absence of sulfur in the final g-C_3N_4 polymer.[13] The role of sulfur is to act as a mediator to modify the electronic band structure of the carbon nitride photocatalyst. Compared to the structure of C_3N_4, the periodic framework of PI looks like the network of C_3N_4 in which three electron-deficient pyromellitic dianhydride blocks have been incorporated,[3] which leads to the electronic deficiency of the triazine ring. The larger radius and lower electronegativity of sulfur (1.84 Å and 2.58, respectively) versus those of N (1.71 Å and 3.04, respectively) endow it with electronic donor properties.[24] Thus, the successful substitution of sulfur for the lattice nitrogen of the triazine ring in the SPI sample is suggested because of the increase in the density of the delocalized π electron in the triazine ring. In addition, the lower polymerization temperature of 325 °C and the existence of acidic dianhydride make the sulfur doping in the framework of PI facile.

The influence of sulfur doping on the chemical state of N in the structure of PI was further investigated by N1s XPS. Figure 5B illustrates the N1s XPS spectra of PI and 25SPI composites. The N1s peak at ∼398.0 eV corresponds to the pyridine-like

Scheme 1. Synthesis of SPI by Polymerization of MA and PMDA at 598 K

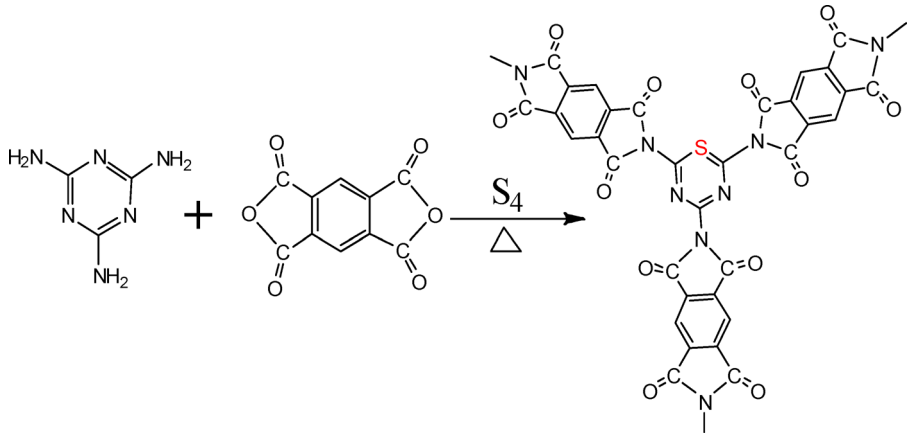

dx.doi.org/10.1021/am500007u | ACS Appl. Mater. Interfaces 2014, 6, 4321−4328

nitrogen atoms in the triazine ring of PI,[25,26] and the shoulder peak at ~399.4 eV is attributed to the nitrogen atoms connecting with two carbonyl (−C═O) groups in the five-membered NC_4 ring (the black curve in Figure 5B).[26] For the sulfur-doped 25SPI sample, the peak at 398.0 eV shifts to a low binding energy of 397.8 eV, implying the electronic density around the nitrogen atom of the triazine ring increases. Notably, the peak at 399.4 eV splits into two new peaks that appear at binding energies of 398.8 and 399.2 eV, indicating two kinds of N arise from the incorporation of sulfur into the triazine ring of PI, which also changes the chemical environment of the nitrogen atom in the neighbor five-membered NC_4 ring.

To improve our understanding of the effect of sulfur doping on the π electron distribution in the 2D framework of PI, we investigated the distribution of electrostatic potential (ESP) on the surface of PI and SPI by using their cluster models. As shown in Figure 6, the most negative and positive surface electrostatic potentials are colored red and blue, respectively. Via comparison of the ESP of PI and SPI, it can be found that the color of the triazine ring in the PI model is very deep (blue), while for the SPI model, the color of the triazine ring moiety is very light (cyan), meaning the substitution of the S atom for the N atom of the triazine ring causes its in-planar electrostatic potential to be more negative. This increase in electronic density is consistent with the N1s XPS results of SPI, in which the characteristic N1s signal of the triazine ring shifted to a low binding energy. The ESP of SPI in Figure 6 (bottom) shows the color of the remaining region around the triazine ring became light, indicating that sulfur doping in PI changes the distribution of the electrostatic potential not only in the triazine ring but also in three neighboring five-membered NC_4 rings. As shown in Figure 6, the distance between the doped sulfur and three N atoms of neighboring five-membered NC_4 rings is different, which results in a nonuniform distribution of negative charge in three N atoms. Correspondingly, two N atoms near the sulfur atom could share negative charge and possess a lower N1s binding energy (398.8 eV), while the other shows a higher binding energy (399.2 eV), as displayed in Figure 5.

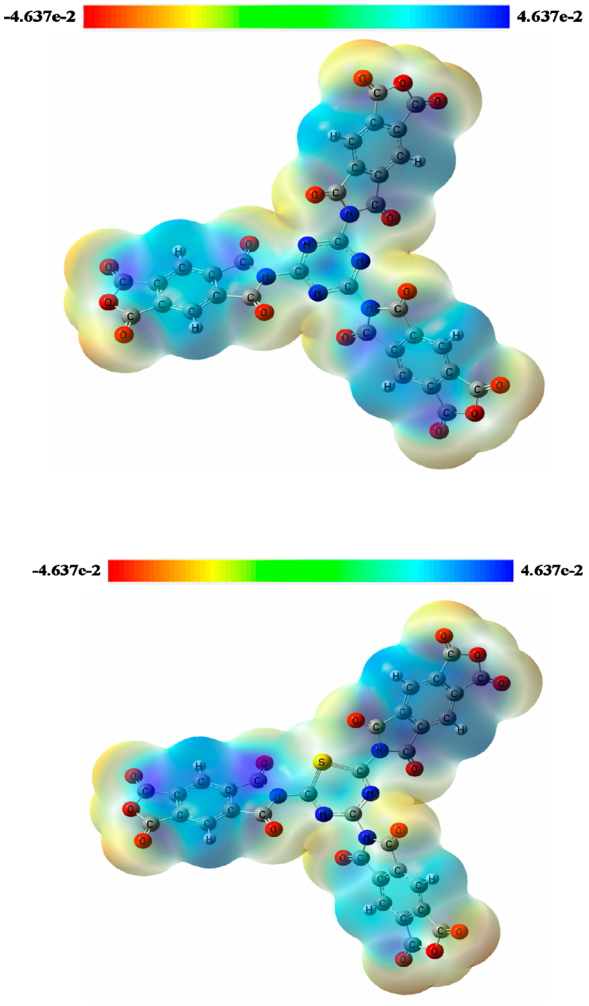

Figure 6. Calculated electronic densities of PI (top) and 25SPI (bottom) samples. Carbon, nitrogen, oxygen, and sulfur in the structural models are shown as gray, blue, red, and yellow spheres, respectively.

Photocatalytic activities of PI and SPI samples were evaluated by the degradation of MO in solution (4 mg/L). As shown in Figure 7A, photolysis of MO under visible light irradiation is negligible in the absence of a photocatalyst. Similarly, the controlled experiment confirms that almost no degradation of MO happens on 25SPI in the dark even after 8 h. Only when the sample was irradiated with visible light was a different degradation activity for MO obtained on PI and sulfur-doped

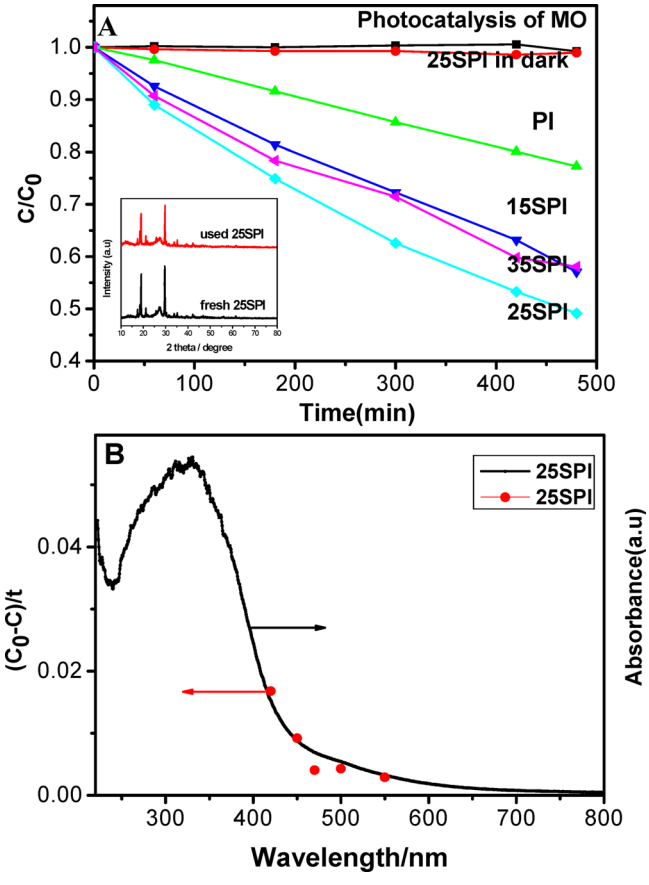

Figure 7. (A) Photodegradation of methyl orange in solution by PI, 15SPI, 25SPI, and 35SPI samples under visible light (λ > 420 nm) irradiation. The inset shows XRD patterns of used and fresh 25SPI samples. (B) Dependence of degradation activity of 25SPI on wavelength.

dx.doi.org/10.1021/am500007u | ACS Appl. Mater. Interfaces 2014, 6, 4321−4328

PI, indicating the degradation of MO on these samples is indeed driven by visible light. The wavelength dependence experiment (Figure 7b) further confirmed the direct correlation between the energy of the irradiated light and the activity of the 25SPI sample; the activity trend is consistent with its absorption edge. For Figure 7, it is noted that all sulfur-doped PI composites show an activity higher than that of pristine PI. The degradation activity of SPI increases with the doping amount of sulfur and reached a maximum for 25SPI; further addition of sulfur to a concentration of 35 wt % in the initial synthesis system caused a decrease in catalytic activity. Among the sulfur-doped samples, 25SPI demonstrated the best performance, which is ~3 times higher than that of PI. Although the actual doping amount of sulfur in the final sample is very limited, that is, 0.24, 0.38, and 0.4 atom % for 15SPI, 25SPI, and 35SPI, respectively, the improvement in the photocatalytic performance of PI caused by sulfur doping is very remarkable. As for the decrease in the photocatalytic activity of 35SPI, it is likely that the sulfur-mediated synthesis of SPI has an optimal doping amount; excess sulfur may led to some structural defects that can act as the recombination centers of the photogenerated electron and hole to weaken the permanence of photocatalysis.

For assessing the durability of this new photocatalyst, the 25SPI sample was also collected after it had been used in photodegradation, and its XRD pattern was compared with that of fresh 25SPI (Figure 7, inset). No distinct difference was observed, which demonstrates the stability of the catalyst and implies its recyclability.

The effect of sulfur doping on the photoabsorption of the PI polymer semiconductor was evaluated by UV–vis. As displayed in Figure 8A, the incorporation of different amounts of sublimed sulfur into PI enhances the harvesting of the samples under visible light, and the sulfur-mediated polyimide has a visible light absorption range wider than that of PI. The absorption edge of PI is nearly at 480 nm, but SPI samples extend the absorption edge to around 600 nm. Meanwhile, the photographs of PI and 25SPI also demonstrate their different colors. Compared with the yellow color of PI, the color of 25SPI is very deep (inset in Figure 8). It is known that the visible light response of PI is ascribed to the excitation of the conjugated π electron from its molecular structure.[3] As mentioned above, the substitution of sulfur for nitrogen in the triazine ring of PI produces an increase in the electron density of the triazine ring, which is favorable for the enlargement of the π electron conjugation of the whole periodic framework of the PI polymer and the extension of the light absorption to the visible region. Moreover, sulfur doping in PI not only shifts its adsorption edge forward toward visible light direction but also changes the transition of charge carriers. As shown in Figure 8B, the PL intensity of 25SPI is weaker than that of PI, indicating the recombination of electron–hole pairs is suppressed effectively. Therefore, the high photocatalytic activity of 25SPI benefits from the high separation efficiency of the photoinduced electron and hole.

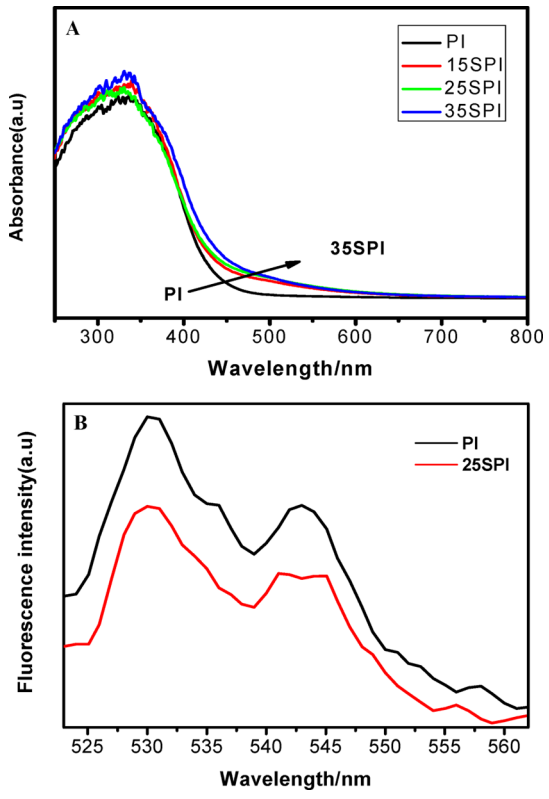

Figure 8. (A) UV–visible spectra of PI and SPI samples. (B) Fluorescence spectra of PI and 25SPI.

It is well-known that the reduction ability of the photoinduced electron and the oxidation ability of the photoinduced hole are relevant to the energy level of CB and VB.[27] The maximum of the valence band can be determined by VBXPS.[28] To further judge the change in the electronic band structure in PI after sulfur doping, the VBXPS spectra of both PI and 25SPI samples were recorded and are illustrated in Figure 9. As shown in Figure 9, the trend of the VB of 25SPI obviously shifts toward a large binding energy, although a noise error existed. The VB binding energy of PI is 0.9 eV, while that of 25SPI is 1.6 eV, which implies the sulfur doping in the framework of PI enhances the oxidation ability of the photoinduced hole of PI. This accounts well for the stronger photocatalytic performance of SPI in the degradation of MO. Although the atomic concentration of sulfur doped in 25SPI is limited to only 0.38 atom %, based on XPS analysis, the modification of sulfur doping for the energy band structure of PI is very effective. Such a downshift effect of VB was also found on the sulfur-mediated carbon nitride (CNS); only 0.5 wt % sulfur doping in the carbon nitride polymer could lower the energy level of VB

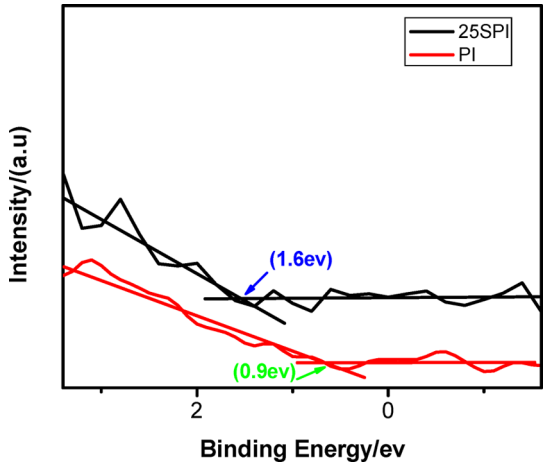

Figure 9. VBXPS spectra of 25SPI and PI.

dx.doi.org/10.1021/am500007u | ACS Appl. Mater. Interfaces 2014, 6, 4321–4328

~0.2 V and correspondingly improved its photocatalytic oxidation for water.[10]

There is speculation that the formation of the C−S bond in the triazine ring of PI via substitution of the C−N bond lowers the top of the VB of PI, which is similar to what has been reported for polythiophen in which the C−S heterocyclic conjugated structure has narrower bandgaps and lower HOMO levels than polypyrrole with the C−N heterocyclic conjugated structure.[29] It is well-known that HOMO and LUMO orbitals in a cluster are the counterparts of VB and CB in a material.[30] In our previous work, the HOMO orbital in the band structure of PI was found to be located in the triazine ring moiety and the LUMO orbital was on the PMDA moiety; the strong electron withdrawal of PMDA resulted in a larger downshift of the VB compared with that of g-C_3N_4.[31] We can conclude that sulfur doping in the triazine ring of the PI sample further promotes this electron pull−push effect and thus lowers its VB level by 0.7 eV, which determines the excellent photocatalytic oxidation performance.

4. CONCLUSION

In summary, we adopted an *in situ* thermal copolymerization method to synthesize a novel sulfur-doped polyimide semiconductor SPI that possesses high activity in the photodegradation of MO in solution. Sulfur doping not only extends the absorption range of PI for visible light but also enhances the oxidation ability of the photoinduced hole, although a small amount of sulfur is incorporated into PI. The doped sulfur substitutes for the nitrogen in triazine rings of PI to form S−C bonds and changes the distribution of negative charge in the 2D plane of PI.

AUTHOR INFORMATION

Corresponding Author

*E-mail: wangy@nju.edu.cn.

Notes

The authors declare no competing financial interest.

ACKNOWLEDGMENTS

This work was financially supported by NSFC (21273111, 21273106, and 51272101), the National Basic Research Program of China (973 Program, 2013CB632404), and the Jiangsu Provincial Natural Science Foundation (BK20130053). We thank the Analysis Center and High Performance Computing Center of Nanjing University for sample characterization and theoretical calculations.

REFERENCES

(1) Wang, X.; Maeda, K.; Thomas, A.; Takanabe, K.; Xin, G.; Carlsson, J. M.; Domen, K.; Antonietti, A. Metal-Free Polymeric Photocatalyst for Hydrogen Production from Water Under Visible Light. *Nat. Mater.* **2009**, *8*, 76−80.

(2) Zhang, J. S.; Zhang, G. G.; Chen, X. F.; Lin, S.; Mçhlmann, L.; Dołega, G.; Lipner, G.; Antonietti, M.; Blechert, S.; Wang, X. C. Co-Monomer Control of Carbon Nitride Semiconductors to Optimize Hydrogen Evolution with Visible Light. *Angew. Chem., Int. Ed.* **2012**, *51*, 3183−3187.

(3) Chu, S.; Wang, Y.; Guo, Y.; Zhou, P.; Yu, H.; Luo, L.; Kong, F.; Zou, Z. G. Facile Green Synthesis of Crystalline Polyimide Photocatalyst for Hydrogen Generation from Water. *J. Mater. Chem.* **2012**, *22*, 15519−15521.

(4) Guo, Y.; Chu, S.; Yan, S. C.; Wang, Y.; Zou, Z. G. Developing a Polymeric Semiconductor Photocatalyst with Visible Light Response. *Chem. Commun.* **2010**, *46*, 7325−7327.

(5) Zhang, Y. J.; Mori, T.; Ye, J. H.; Antonietti, M. Phosphorus-Doped Carbon Nitride Solid: Enhanced Electrical Conductivity and Photocurrent Generation. *J. Am. Chem. Soc.* **2010**, *132*, 6294−6295.

(6) Wang, Y.; Di, Y.; Antonietti, M.; Li, H. R.; Chen, X. F.; Wang, X. C. Excellent Visible-Light Photocatalysis of Fluorinated Polymeric Carbon Nitride Solids. *Chem. Mater.* **2010**, *22*, 5119−5121.

(7) Liu, G.; Niu, P.; Sun, C.; Smith, S. C.; Chen, Z.; Lu, G. Q. (M.); Cheng, H.-M. Unique Electronic Structure Induced High Photoreactivity of Sulfur-Doped Graphitic C_3N_4. *J. Am. Chem. Soc.* **2010**, *132*, 11642−11648.

(8) Hong, J. D.; Xia, X. Y.; Wang, Y. S.; Xu, R. Mesoporous Carbon Nitride with *in situ* Sulfur Doping for Enhanced Photocatalytic Hydrogen Evolution from Water Under Visible Light. *J. Mater. Chem.* **2012**, *22*, 15006−15012.

(9) Zhang, Z. Z.; Long, J. L.; Yang, L. F.; Chen, W. K.; Dai, W. X.; Fu, X. Z.; Wang, X. X. Organic Semiconductor for Artificial Photosynthesis: Water Splitting into Hydrogen by a Bioinspired $C_3N_3S_3$ Polymer under Visible Light Irradiation. *Chem. Sci.* **2011**, *2*, 1826−1830.

(10) Zhang, J. S.; Sun, J. H.; Maeda, K.; Domen, K.; Liu, P.; Antonietti, M.; Fu, X. Z.; Wang, X. C. Sulfur-mediated Synthesis of Carbon Nitride: Band-gap Engineering and Improved Functions for Photocatalysis. *Energy Environ. Sci.* **2011**, *4*, 675−678.

(11) Zhang, G. G.; Zhang, J. S.; Zhang, M. W.; Wang, X. C. Polycondensation of Thiourea into Carbon Nitride Semiconductors as Visible Light Photocatalysts. *J. Mater. Chem.* **2012**, *22*, 8083−8091.

(12) Cui, Y. J.; Zhang, J. S.; Zhang, G. G.; Huang, J. H.; Liu, P.; Antonietti, M.; Wang, X. C. Synthesis of Bulk and Nanoporous Carbon Nitride Polymers from Ammonium Thiocyanate for Photocatalytic Hydrogen Evolution. *J. Mater. Chem.* **2011**, *21*, 13032−13039.

(13) Zhang, J. S.; Zhang, M. W.; Zhang, G. G.; Wang, X. C. Synthesis of Carbon Nitride Semiconductors in Sulfur Flux for Water Photoredox Catalysis. *ACS Catal.* **2012**, *2*, 940−948.

(14) Goettmann, F.; Fischer, A.; Antonietti, M.; Thomas, A. Chemical Synthesis of Mesoporous Carbon Nitrides Using Hard Templates and Their Use as a Metal-Free Catalyst for Friedel−Crafts Reaction of Benzene. *Angew. Chem., Int. Ed.* **2006**, *45*, 4467−4471.

(15) Zeng, S. Z.; Guo, L. M.; Cui, F. M.; Gao, Z.; Zhou, J.; Shi, J. L. In situ Self-Assembly of Zigzag Polyimide Chains to Crystalline Branched Supramolecular Structures with High Surface Area. *Macromol. Chem. Phys.* **2010**, *211*, 698−705.

(16) Park, S. J.; Li, K.; Jin, F. L. Synthesis and Characterization of Hyper-branched Polyimides from 2,4,6-triaminopyrimidine and Dianhydrides System. *Mater. Chem. Phys.* **2008**, *108*, 214−219.

(17) Manecke, G.; Wöhrle, D. Syntheses und Halbleitereigenschaften Einiger Komplexe under aus Ihnen Hergestellten Polymeren. Teil 2. Polymere mit Phthalocyaninartiger und Triazinartiger Stuktur. *Macromol. Chem. Phys.* **1968**, *120*, 176−191.

(18) Niu, P.; Zhang, L. L.; Liu, G.; Cheng, H. M. Graphene-Like Carbon Nitride Nanosheets for Improved Photocatalytic Activities. *Adv. Funct. Mater.* **2012**, *22*, 4763−4770.

(19) Bojdys, M. J.; Wohlgemuth, S. A.; Thomas, A.; Antonietti, M. Ionothermal Route to Layered Two- Dimensional Polymer-Frameworks Based on Heptazine Linkers. *Macromolecules* **2010**, *43*, 6639−6645.

(20) Ma, W. S.; Zeng, X. R.; Gong, K. C. Characterization of Polyaniline/Thiokol Rubber Composite Films (I). *Huanan Ligong Daxue Xuebao, Ziran Kexueban* **1999**, *27*, 12−17.

(21) Lindberg, B. J.; Hamrin, K.; Johansson, G.; Gelius, U.; Fahlmann, A.; Nordling, C.; Siegbahn, K. Molecular Spectroscopy by Means of ESCA II. Sulfur compounds. Correlation of Electron Binding Energy with Structure. *Phys. Scr.* **1970**, *1*, 286−298.

(22) Ge, L.; Han, C. C.; Xiao, X. L.; Guo, L. L.; Li, Y. J. Enhanced Visible Light Photocatalytic Hydrogen Evolution of Sulfur-doped Polymeric g-C_3N_4 Photocatalysts. *Mater. Res. Bull.* **2013**, *48*, 3919−3925.

(23) Kunio, M.; Suzuki, K.; Shimizu, K.; Oishi, Y. Evaporation Polymerization of Dibutylamino 1,3,5-triazine-2,4-dithiol on Iron Plates. *Langmuir* **2002**, *18*, 9527−9532.

(24) Liu, G.; Wang, L. Z.; Yang, H. G.; Cheng, H. M.; Lu, G. Q. Titania-based Photocatalysts Cystal Growth, Doping and Heterostructuring. *J. Mater. Chem.* **2010**, *20*, 831−843.
(25) Guo, Y.; Kong, F.; Chu, S.; Luo, L. L.; Yang, J. C.; Wang, Y.; Zou, Z. G. Simultaneous Sensitization and Hole Activation in Carbon Nitride Polymer Sensitized TiO_2. *RSC Adv.* **2012**, *2*, 5585−5590.
(26) Yang, J. C.; Chu, S.; Guo, Y.; Luo, L. L.; Kong, F.; Wang, Y.; Zou, Z. G. Hyperbranched Polymeric N-oxide: A Novel Kind of Metal-free Photocatalyst. *Chem. Commun.* **2012**, *48*, 3533−3535.
(27) Linsebigler, A. L.; Lu, G.; Yates, J. T. Photocatalysis on TiO_2 Surfaces: Principles, Mechanisms, and Selected Results. *Chem. Rev.* **1995**, *95*, 735−758.
(28) Chen, X. B.; Liu, L.; Peter, Y.; Mao, S. S. Increasing Solar Absorption for Photocatalysis With Black Hydrogenated Titanium Dioxide Nanocrystals. *Science* **2011**, *331*, 746−749.
(29) Ma, J.; Li, S.; Jiang, Y. A.; Time-Dependent, D. F. T. Study on Band Gaps and Effective Conjugation Lengths of Polyacetylene, Polyphenylene, Polypentafulvene, Polycyclopentadiene, Polypyrrole, Polyfuran, Polysilole, Polyphosphole, and Polythiophene. *Macromolecules* **2002**, *35*, 1109−1115.
(30) Qu, Z. W.; Kroes, G. J. Theoretical Study of the Electronic Structure and Stability of Titanium Dioxide Clusters $(TiO_2)_n$ with n = 1−9. *J. Phys. Chem. B* **2006**, *110*, 8998−9007.
(31) Chu, S.; Wang, Y.; Guo, Y.; Feng, J. Y.; Wang, C. C.; Luo, W. J.; Fan, X. X.; Zou, Z. G. Band Structure Engineering of Carbon Nitride: In Search of a Polymer Photocatalyst with High Photooxidation Property. *ACS Catal.* **2013**, *3*, 912−919.